

J. E. H. Sansom · E. Kendrick · J. R. Tolchard ·
M. S. Islam · P. R. Slater

A comparison of the effect of rare earth vs Si site doping on the conductivities of apatite-type rare earth silicates

Received: 11 January 2006 / Accepted: 24 January 2006 / Published online: 21 April 2006
© Springer-Verlag 2006

Abstract Apatite-type lanthanum silicate ($\text{La}_{9.33}\text{Si}_6\text{O}_{26}$) has been attracting significant recent interest due to its high oxide ion conductivity. In this paper, synthesis and conductivity data for a range of doped samples (Mg, Ca, Sr, Ba, B, Ga and Zn) are reported, in particular, to compare the effect of rare earth vs Si site doping. The results show that Ga, B and Zn favour substitution on the Si site, while Ca, Sr and Ba favour La-site substitution. Mg is shown to be an ambi-site dopant, substituting on either site depending on the starting composition. The samples doped on the Si site show higher conductivities than comparable samples doped on the La site, providing further support for the importance of the silicate network in the conduction process, as initially predicted by atomistic modelling studies. For Ga doping on the Si site, the effect of varying the rare-earth size on the conductivities is also reported.

Keywords Apatite · Oxide ion conduction · Dopant · Rare earth

Introduction

Research on oxide ion conducting materials has dramatically increased over the past few decades. This can be

J. E. H. Sansom · E. Kendrick · P. R. Slater (✉)

Chemistry, UniS Materials Institute,
University of Surrey, Guildford,
Surrey, GU2 7XH, UK

e-mail: p.slater@surrey.ac.uk

Tel.: +44-1483-686847

Fax: +44-1483-686851

J. R. Tolchard
Department of Materials Technology,
Norwegian University of Science and Technology, Sem
Sælands vei 14,
N-7491 Trondheim, Norway

M. S. Islam
Department of Chemistry, University of Bath,
Bath, BA2 7AY, UK

correlated with their importance in a range of technological applications, such as fuel cells, oxygen sensors and separation membranes. In particular, interest in developing improved electrolytes for use in solid oxide fuel cells (SOFCs) has driven much of this research interest. Most SOFC electrolyte work has focused on materials with fluorite (e.g. doped ZrO_2 , CeO_2) or perovskite (e.g. doped LaGaO_3)-related structures [1]. Such materials are typically doped with aliovalent cations to introduce oxygen vacancies, and oxide ion conduction can then proceed via these vacant sites.

The detailed research on fluorite and perovskite systems has essentially reached the state of the art that can be achieved in such structures. Therefore, the search for new electrolytes has now begun to target alternative structure types, and, in this respect, the apatite structure has attracted significant interest. Research in this area has grown after the initial reports by Nakayama et al. of high oxide ion conductivity ($>10^{-3} \text{ Scm}^{-1}$ at 500°C) in $\text{Ln}_{10-x}\text{Si}_6\text{O}_{26+y}$ (Ln =rare earth) [2–9]. More recently, even higher oxide ion conductivities have been observed in Ge-based analogues, i.e. $\text{Ln}_{10-x}\text{Ge}_6\text{O}_{26+y}$, although these particular materials suffer from Ge volatility problems on synthesis/sintering [10–15]. The structure of these apatite systems is shown in Fig. 1. It consists of isolated Si/GeO_4 units with the rare-earth cations located in nine coordinate and seven coordinate cavity sites. The extra oxide ions occupy one-dimensional channels running through the structure.

In contrast to the perovskite/fluorite-type oxide ion conductors, where oxide ion conduction proceeds via oxygen vacancies, these apatite-type materials are believed to conduct via an interstitial mechanism. The presence of oxygen interstitials and, therefore, high conductivity is favoured for samples containing oxygen excess, e.g. $\text{La}_9\text{BaSi}_6\text{O}_{26.5}$, and/or cation vacancies, e.g. $\text{La}_{9.33}\text{Si}_6\text{O}_{26}$. In contrast, samples which are fully stoichiometric, e.g. $\text{La}_8\text{Ba}_2\text{Si}_6\text{O}_{26}$, show poor conductivity due to lack of interstitial oxygens [9, 16–18].

Key results that aid in understanding the conduction mechanism in these apatite-type systems have been obtained from computer modelling and neutron powder

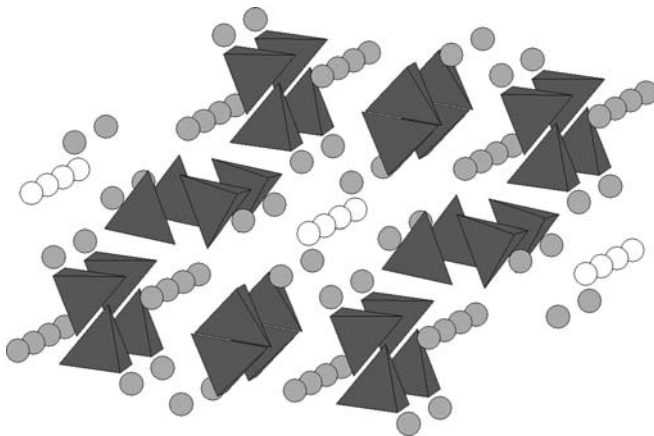


Fig. 1 The structure of the apatite-type oxide ion conductors, $\text{La}_{10-x}(\text{Si}/\text{GeO}_4)_6\text{O}_{2+y}$ (dark spheres=La, tetrahedra= Si/GeO_4 , light spheres=O)

diffraction studies. The modelling studies identified a new energetically favourable interstitial oxide ion position at the periphery of the oxide ion channels in the vicinity of the SiO_4 groups [19, 20]. The presence of this interstitial oxygen site has been subsequently confirmed by neutron diffraction experiments [21–23]. Moreover, the modelling further suggested a complex sinusoidal conduction pathway down the channels, aided by the cooperative displacements of the silicate substructure (Fig. 2) [19, 20]. Experimental support for the importance of the silicate substructure includes the high thermal displacement parameters for the silicate oxygens observed in structural studies of these materials, and results from solid state ^{29}Si NMR studies. In terms of the latter, these NMR studies have shown a correlation between the silicon environment and the observed conductivity [24]. Specifically, samples that show poor conductivity (i.e. fully stoichiometric samples, such as $\text{La}_8\text{Ba}_2\text{Si}_6\text{O}_{26}$) demonstrate a single NMR resonance, whereas, fast-ion conducting compositions (i.e. samples containing cation vacancies and/or oxygen excess, for example $\text{La}_{9.33}\text{Si}_6\text{O}_{26}$ and $\text{La}_9\text{BaSi}_6\text{O}_{26.5}$) show two or three.

One of the key features of these apatite-type oxides, with respect to further optimisation of their conductivities, is the wide range of doping possibilities within the structure. Previous studies have suggested that for oxygen stoichiometric samples, doping onto the Si site with small levels of lower valent ions ($\text{La}_{9.33+x/3}\text{Si}_{6-x}\text{M}_x\text{O}_{26}$; M=B, Al, Ga, Fe, Mn, Co) enhances the conductivity, whereas, a similar doping strategy ($\text{La}_{9.33-2x/3}\text{M}_x\text{Si}_6\text{O}_{26}$; M=Mg, Ca, Sr, Ba) on the La site results in a general reduction in the conductivity [9, 16–32]. This has been correlated with the modelling predictions of the importance of the silicate network in aiding the conduction down the channels.

In this paper, we summarise our previous results and report an investigation on the incorporation of further dopants into the apatite structure, comparing the results with predictions from atomistic modelling studies. Conductivities are reported and discussed for successfully doped samples. A key focus is the effect of rare-earth vs Si

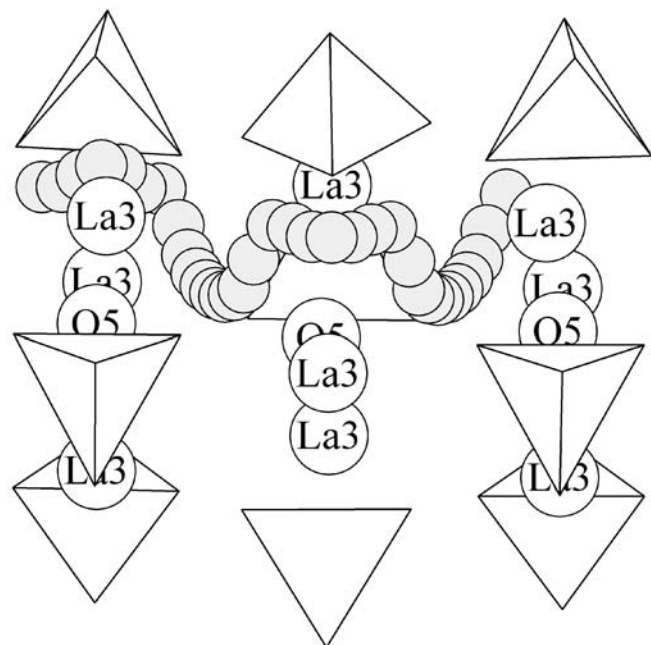


Fig. 2 The proposed mechanism of interstitial oxide ion migration in $\text{La}_{9.33}\text{Si}_6\text{O}_{26}$, viewed perpendicular to the oxide ion channel

site doping, particularly relating to dopants that can substitute on both sites, e.g. Mg. In addition, the effect of varying the rare-earth size in samples doped with Ga on the Si site is discussed.

Materials and methods

The undoped rare earth silicates, $\text{Ln}_{9.33}\text{Si}_6\text{O}_{26}$ (Ln=La, Pr, Nd, Sm, Eu, Gd) were prepared from high purity La_2O_3 , Pr_6O_{11} , Nd_2O_3 , Sm_2O_3 , Eu_2O_3 , Gd_2O_3 , and SiO_2 . The powders in the correct stoichiometric ratio were intimately mixed and heated to 1300°C for 16 h. The samples were then reground and reheated at 1350°C for another 16 h. Phase purity was determined by X-ray diffraction (Seifert 3003TT X-ray diffractometer). Dense (>90% theoretical) pellets for conductivity measurements were prepared by pressing 1.3-cm diameter pellets and sintering at 1550–1650°C. Conductivity measurements were performed using ac impedance spectroscopy (Hewlett Packard 4192A Impedance Analyser or Solartron 1260 Impedance Analyser).

In terms of doping studies, the following dopants were examined: Mg, Ca, Sr, Ba, Zn, B, Ga, In, Cr, Sc, Sn, Nb and W. Initial work focussed on doping the $\text{La}_{9.33}\text{Si}_6\text{O}_{26}$ system, maintaining a constant oxygen stoichiometry. The following doping strategies were investigated with the dopant starting material employed given in brackets:

- $\text{La}_{9.33-2x/3}\text{Mg}_x\text{Si}_6\text{O}_{26}$, $\text{La}_{9.33+2x/3}\text{Si}_{6-x}\text{Mg}_x\text{O}_{26}$, $\text{La}_{9.33}\text{Mg}_x\text{Si}_{6-x}\text{Mg}_x\text{O}_{26}$ (MgO),
- $\text{La}_{9.33-2x/3}\text{Ca}_x\text{Si}_6\text{O}_{26}$, $\text{La}_{9.33+2x/3}\text{Si}_{6-x}\text{Ca}_x\text{O}_{26}$ (CaCO_3),
- $\text{La}_{9.33-2x/3}\text{Sr}_x\text{Si}_6\text{O}_{26}$ (SrCO_3),
- $\text{La}_{9.33-2x/3}\text{Ba}_x\text{Si}_6\text{O}_{26}$ (BaCO_3),

- $\text{La}_{9.33-2x/3}\text{Zn}_x\text{Si}_6\text{O}_{26}$, $\text{La}_{9.33+2x/3}\text{Si}_{6-x}\text{Zn}_x\text{O}_{26}$ (ZnO)
- $\text{La}_{9.33+x/3}\text{Si}_{6-x}\text{B}_x\text{O}_{26}$ (H_3BO_3)
- $\text{La}_{9.33-x}\text{Ga}_x\text{Si}_6\text{O}_{26}$, $\text{La}_{9.33+x/3}\text{Si}_{6-x}\text{Ga}_x\text{O}_{26}$ (Ga_2O_3),
- $\text{La}_{9.33-x}\text{In}_x\text{Si}_6\text{O}_{26}$, $\text{La}_{9.33+x/3}\text{Si}_{6-x}\text{In}_x\text{O}_{26}$ (In_2O_3),
- $\text{La}_{9.33-x}\text{Cr}_x\text{Si}_6\text{O}_{26}$, $\text{La}_{9.33+x/3}\text{Si}_{6-x}\text{Cr}_x\text{O}_{26}$ (Cr_2O_3),
- $\text{La}_{9.33-x}\text{Sc}_x\text{Si}_6\text{O}_{26}$, $\text{La}_{9.33+x/3}\text{Si}_{6-x}\text{Sc}_x\text{O}_{26}$ (Sc_2O_3),
- $\text{La}_{9.33-4x/3}\text{Sn}_x\text{Si}_6\text{O}_{26}$, $\text{La}_{9.33}\text{Si}_{6-x}\text{Sn}_x\text{O}_{26}$ (SnO_2),
- $\text{La}_{9.33-5x/3}\text{Nb}_x\text{Si}_6\text{O}_{26}$, $\text{La}_{9.33-x/3}\text{Si}_{6-x}\text{Nb}_x\text{O}_{26}$ (Nb_2O_5),
- $\text{La}_{9.33-2x/3}\text{Si}_{6-x}\text{W}_x\text{O}_{26}$ (WO_3).

In addition to the doping studies listed above, three dual doped samples were prepared to examine the combined effect of dopants, $\text{La}_{9.33}\text{Ba}_{0.5}\text{Si}_{5.5}\text{Mg}_{0.5}\text{O}_{26}$, $\text{La}_{9.83}\text{Si}_5\text{M}_{0.5}\text{Mg}_{0.5}\text{O}_{26}$ ($\text{M}=\text{B}, \text{Ga}$).

Furthermore, in the case of Mg and Ga doping on the Si site, the effect of varying the rare-earth cation size was also investigated; i.e. the preparation and characterisation of $\text{Ln}_{9.67}\text{Si}_5\text{GaO}_{26}$, $\text{Ln}_{9.5}\text{Si}_{5.75}\text{Mg}_{0.25}\text{O}_{26}$ ($\text{Ln}=\text{La, Pr, Nd, Sm, Eu, Gd}$).

The doped samples were prepared from intimate mixtures of the starting materials in the correct stoichiometric ratio, with an initial heat treatment of 1300°C for 16 h (for Boron-doped samples, a pre-treatment at 250°C for 2 h was employed). The samples were then reground and reheated to 1350–1500°C for another 16 h. Phase purity was determined by X-ray diffraction (Seifert 3003TT X-ray diffractometer).

Pellets for conductivity measurements were prepared similarly to the undoped phases. In the case of Boron doping, slightly lower sintering temperatures of 1450–

1600 °C were employed (the lower temperatures for the higher B contents).

Results and discussion

Of the dopants examined, X-ray diffraction results showed no evidence for any successful incorporation of In, Cr, Sc, Sn, Nb and W into $\text{La}_{9.33}\text{Si}_6\text{O}_{26}$. In addition, Zn and Ga substitution on the La site were shown to be unsuccessful, as was Ca doping on the Si site. In terms of successful dopants, these are summarised below:

- La site: Mg, Ca, Sr, Ba
- Si site: B, Ga, Zn, Mg

From this, it is interesting to note that Mg is an ambi-site dopant, able to substitute on both the La and Si sites.

The results follow modelling predictions in terms of larger dopants favouring the La site, with smaller dopants favouring the Si site [33]. In addition, the results confirm the modelling conclusions that the structure can accommodate dopants covering a wide range of ionic radii (from Ba^{2+} to Mg^{2+} for the La site, and from B^{3+} to Mg^{2+} on the Si site). This ability to allow an unusually broad range of dopants to be incorporated into the structure can be correlated with the flexibility of the structure and, in particular, the silicate substructure, which allows local distortion and alteration of site size [33].

Cell parameters for a range of successfully doped samples are given in Table 1, while bulk conductivities are given in Table 2. The reported cell parameter data are

Table 1 Cell parameters (hexagonal cell) for $\text{La}_{9.33}\text{Si}_6\text{O}_{26}$ doped with Mg, Ca, Sr, Ba, B, Ga and Zn

Sample composition	<i>a</i> (Å)	<i>c</i> (Å)	Dopant site
$\text{La}_{9.33}\text{Si}_6\text{O}_{26}$	9.721(3)	7.187(3)	Undoped
$\text{La}_{8.67}\text{BaSi}_6\text{O}_{26}$	9.757(3)	7.275(3)	La
$\text{La}_{8.33}\text{Ba}_{1.5}\text{Si}_6\text{O}_{26}$	9.768(3)	7.310(3)	La
$\text{La}_8\text{Ba}_2\text{Si}_6\text{O}_{26}$	9.790(2)	7.331(2)	La
$\text{La}_{8.67}\text{SrSi}_6\text{O}_{26}$	9.714(4)	7.220(3)	La
$\text{La}_{8.33}\text{Sr}_{1.5}\text{Si}_6\text{O}_{26}$	9.713(3)	7.234(3)	La
$\text{La}_8\text{Sr}_2\text{Si}_6\text{O}_{26}$	9.708(1)	7.238(1)	La
$\text{La}_{8.67}\text{CaSi}_6\text{O}_{26}$	9.693(3)	7.176(3)	La
$\text{La}_{8.33}\text{Ca}_{1.5}\text{Si}_6\text{O}_{26}$	9.683(3)	7.163(3)	La
$\text{La}_8\text{Ca}_2\text{Si}_6\text{O}_{26}$	9.661(2)	7.155(2)	La
$\text{La}_9\text{Mg}_{0.5}\text{Si}_6\text{O}_{26}$	9.691(1)	7.137(1)	La
$\text{La}_{8.67}\text{MgSi}_6\text{O}_{26}$	9.647(2)	7.092(2)	La
$\text{La}_{9.33}\text{Mg}_{0.5}\text{Si}_{5.5}\text{Mg}_{0.5}\text{O}_{26}$	9.709(1)	7.161(1)	La+Si
$\text{La}_{9.5}\text{Si}_{5.75}\text{Mg}_{0.25}\text{O}_{26}$	9.724(1)	7.194(1)	Si
$\text{La}_{9.67}\text{Si}_{5.5}\text{Mg}_{0.5}\text{O}_{26}$	9.734(1)	7.216(1)	Si
$\text{La}_{9.5}\text{Si}_{5.75}\text{Zn}_{0.25}\text{O}_{26}$	9.724(1)	7.200(1)	Si
$\text{La}_{9.5}\text{Si}_{5.5}\text{Ga}_{0.5}\text{O}_{26}$	9.735(2)	7.214(2)	Si
$\text{La}_{9.67}\text{Si}_5\text{GaO}_{26}$	9.744(1)	7.232(1)	Si
$\text{La}_{9.83}\text{Si}_{4.5}\text{Ga}_{1.5}\text{O}_{26}$	9.759(2)	7.252(2)	Si
$\text{La}_{10}\text{Si}_4\text{Ga}_2\text{O}_{26}$	9.770(1)	7.268(1)	Si
$\text{La}_{9.5}\text{Si}_{5.5}\text{B}_{0.5}\text{O}_{26}$	9.690(3)	7.212(3)	Si
$\text{La}_{9.67}\text{Si}_5\text{BO}_{26}$	9.640(3)	7.212(3)	Si
$\text{La}_{9.83}\text{Si}_{4.5}\text{B}_{1.5}\text{O}_{26}$	9.591(3)	7.213(3)	Si
$\text{La}_{10}\text{Si}_4\text{B}_2\text{O}_{26}$	9.552(3)	7.219(3)	Si

all in agreement with those expected from the dopant size. For example, doping Mg onto the La site ($\text{La}_9\text{Mg}_{0.5}\text{Si}_6\text{O}_{26}$) results in a significant decrease in cell size due to the smaller size of Mg^{2+} compared to La^{3+} . In contrast, substitution on the Si site ($\text{La}_{9.67}\text{Si}_{5.5}\text{Mg}_{0.5}\text{O}_{26}$) results in an increase in the cell size as Mg^{2+} is larger than Si^{4+} . The sample doped with Mg on both sites ($\text{La}_{9.33}\text{Mg}_{0.5}\text{Si}_{5.5}\text{Mg}_{0.5}\text{O}_{26}$) has cell parameters in-between these two samples. The conductivity data will now be discussed with relevance to La vs Si site substitution.

Comparison of the effect of doping on the La vs the Si site in $\text{La}_{9.33}\text{Si}_6\text{O}_{26}$

Doping $\text{La}_{9.33}\text{Si}_6\text{O}_{26}$ on the Si site with lower valent ions (B^{3+} , Ga^{3+} , Mg^{2+} , Zn^{2+}), while maintaining the oxygen stoichiometry at 26, requires an increase in the La content and, hence, a reduction in the number of cation vacancies, i.e. $\text{La}_{9.33+x/3}\text{Si}_{6-x}\text{M}_x\text{O}_{26}$ ($\text{M}=\text{B}$, Ga), $\text{La}_{9.33+2x/3}\text{Si}_{6-x}\text{M}_x\text{O}_{26}$ ($\text{M}=\text{Mg}$, Zn). The work on Ga doping, previously reported [30], shows that the conductivity initially increases on increasing substitution and correspondingly reducing the number of La cation vacancies (Table 2), before decreasing as the fully stoichiometric phase, $\text{La}_{10}\text{Si}_4\text{Ga}_2\text{O}_{26}$, is approached. These results are similar to data for Al doping on the Si site reported by Abram et al. [25].

Table 2 Conductivity data for $\text{La}_{9.33}\text{Si}_6\text{O}_{26}$ doped with Mg, Ca, Sr, Ba, B, Ga and Zn

Sample composition	σ (Scm^{-1}) at 500 °C (unless otherwise stated)	E_a (eV)
$\text{La}_{9.33}\text{Si}_6\text{O}_{26}$	1.1×10^{-4}	0.74
$\text{La}_{8.67}\text{BaSi}_6\text{O}_{26}$	1.4×10^{-4}	0.67
$\text{La}_{8.33}\text{Ba}_{1.5}\text{Si}_6\text{O}_{26}$	6.6×10^{-5}	0.75
$\text{La}_8\text{Ba}_2\text{Si}_6\text{O}_{26}$	5.4×10^{-7} (800 °C)	1.21
$\text{La}_{8.67}\text{SrSi}_6\text{O}_{26}$	8.3×10^{-5}	0.87
$\text{La}_{8.33}\text{Sr}_{1.5}\text{Si}_6\text{O}_{26}$	1.3×10^{-5}	0.88
$\text{La}_8\text{Sr}_2\text{Si}_6\text{O}_{26}$	5.6×10^{-7} (800 °C)	1.14
$\text{La}_{8.67}\text{CaSi}_6\text{O}_{26}$	5.8×10^{-5}	0.86
$\text{La}_{8.33}\text{Ca}_{1.5}\text{Si}_6\text{O}_{26}$	3.4×10^{-5}	0.88
$\text{La}_8\text{Ca}_2\text{Si}_6\text{O}_{26}$	9.9×10^{-7} (800 °C)	1.62
$\text{La}_9\text{Mg}_{0.5}\text{Si}_6\text{O}_{26}$	2.1×10^{-5}	0.98
$\text{La}_{8.67}\text{MgSi}_6\text{O}_{26}$	3.6×10^{-6}	1.13
$\text{La}_{9.33}\text{Mg}_{0.5}\text{Si}_{5.5}\text{Mg}_{0.5}\text{O}_{26}$	1.6×10^{-4}	0.80
$\text{La}_{9.5}\text{Si}_{5.75}\text{Mg}_{0.25}\text{O}_{26}$	1.8×10^{-3}	0.68
$\text{La}_{9.67}\text{Si}_{5.5}\text{Mg}_{0.5}\text{O}_{26}$	3.0×10^{-3}	0.67
$\text{La}_{9.5}\text{Si}_{5.75}\text{Zn}_{0.25}\text{O}_{26}$	2.1×10^{-3}	0.71
$\text{La}_{9.5}\text{Si}_{5.5}\text{Ga}_{0.5}\text{O}_{26}$	4.6×10^{-4}	0.67
$\text{La}_{9.67}\text{Si}_5\text{GaO}_{26}$	1.0×10^{-3}	0.70
$\text{La}_{9.83}\text{Si}_{4.5}\text{Ga}_{1.5}\text{O}_{26}$	1.3×10^{-3}	0.73
$\text{La}_{10}\text{Si}_4\text{Ga}_2\text{O}_{26}$	4.1×10^{-6}	0.72
$\text{La}_{9.5}\text{Si}_{5.5}\text{B}_{0.5}\text{O}_{26}$	4.1×10^{-4}	0.69
$\text{La}_{9.67}\text{Si}_5\text{BO}_{26}$	3.3×10^{-4}	0.75
$\text{La}_{9.83}\text{Si}_{4.5}\text{B}_{1.5}\text{O}_{26}$	4.9×10^{-4}	0.73
$\text{La}_{10}\text{Si}_4\text{B}_2\text{O}_{26}$	5.5×10^{-7}	0.98

For B doping, a smaller general increase in conductivity is observed, which may be related to the smaller size of B.

In contrast to the high substitution levels possible for B and Ga doping ($0 \leq x \leq 2$), the doping limits for Mg and Zn substitution onto the Si site, $\text{La}_{9.33+2x/3}\text{Si}_{6-x}\text{M}_x\text{O}_{26}$ ($\text{M}=\text{Mg}$, Zn), are significantly lower, with impurities being observed for $x > 0.5$ (Mg) and $x > 0.25$ (Zn). The conductivity data show, however, that as for B and Ga doping, Mg substitution in place of Si, according to the doping strategy $\text{La}_{9.33+2x/3}\text{Si}_{6-x}\text{Mg}_x\text{O}_{26}$, raises the conductivity, in agreement with recent reports by Yoshioka et al. [34, 35]. However, contrary to these reports, where it was assumed that Mg can only substitute onto the Si site, the results in this paper show that Mg is an ambi-site dopant, allowing both substitution on the La and Si site to be achieved, depending on the starting composition (Table 1). Zn doping on the Si site, reported for the first time in this paper, shows a similar enhancement in conductivity to Mg doping. For both these divalent dopants, it appears as if only very low levels ($x=0.25$, 4.17%) are required to achieve an order of magnitude enhancement in conductivity (Table 2).

The complex change in conductivity on B, Al and Ga doping, with an initial increase in conductivity followed by a substantial decrease for the fully stoichiometric composition, $\text{La}_{10}\text{Si}_4\text{M}_2\text{O}_{26}$ ($\text{M}=\text{B}$, Al, Ga), is interesting. Previously, it was thought that this conductivity behaviour may be explained by the presence of an optimum cation vacancy level in such samples [25, 36]. However, for the comparable doping strategy on the La site, i.e. $\text{La}_{9.33-2x/3}\text{A}_x\text{Si}_6\text{O}_{26}$ ($\text{A}=\text{Mg}$, Ca , Sr , Ba), no such large increase in the conductivity is observed as the number of cation vacancies is decreased. Instead, a general decrease in conductivity is typically observed over the range of samples (Table 2), with the magnitude of the observed change in conductivity being strongly dependent on the size of the dopant cation. Specifically, it seems that the introduction of small cations, e.g. Mg^{2+} , on the La site results in a substantial decrease in conductivity, while the introduction of low levels of larger cations, e.g. Ba^{2+} , produces little change in conductivity.

An explanation for this difference comes from the results of atomistic simulation studies [33]. From such studies, it has been shown that divalent dopants preferentially substitute for the 9-coordinate La site. However, for small divalent cation dopants, e.g. Mg^{2+} , the simulation studies show that considerable distortion of this site occurs on incorporation of the dopant, such that six of the M–O bonds are shortened significantly, while the remaining three M–O bonds undergo significant elongation [33]. The overall effect is that for small dopants on the La site, the coordination environment effectively reduces from 9 to 6 coordination. This dramatic change in local structure is likely to have a significant effect on the tetrahedral silicate framework, perhaps reducing its flexibility and, thus, accounting for the lower conductivity.

The different effects of La vs Si site doping can be clearly seen in Fig. 3, which shows data for samples with the same level of cation vacancies. This figure shows that samples doped on the Si site have significantly higher

conductivities than comparable samples doped on the La site, indicating that the increase in conductivity for the Si site dopants is more likely to be related to the effect of the incorporation of a lower valent cation on the Si site, rather than the reduction in the number of cation vacancies. This is supported by the fact that the conductivities of fully stoichiometric samples with dopants on the Si site, e.g. $\text{La}_{10}(\text{SiO}_4)_4(\text{GaO}_4)_2\text{O}_2$ ($\sigma_{800^\circ\text{C}}=6.81\times10^{-5}$ Scm $^{-1}$), are also significantly higher than for equivalent samples with dopants on the La site, e.g. $\text{La}_8\text{Sr}_2(\text{SiO}_4)_6\text{O}_2$ ($\sigma_{800^\circ\text{C}}=5.64\times10^{-7}$ Scm $^{-1}$).

A particularly striking feature is the large difference in conductivities between Mg-doped samples on the Si and La sites (Table 2, Fig. 3). The results show nearly three-orders-of-magnitude difference in conductivity between the sample doped on the La site ($\text{La}_{8.67}\text{MgSi}_6\text{O}_{26}$) and that doped on the Si site ($\text{La}_{9.67}\text{Si}_{5.5}\text{Mg}_{0.5}\text{O}_{26}$), with the conductivity of the dual-site-doped sample ($\text{La}_{9.33}\text{Mg}_{0.5}\text{Si}_{5.5}\text{Mg}_{0.5}\text{O}_{26}$) lying in-between the two values. This result emphasises the beneficial effect of doping small levels of lower valent cations on the Si site.

Following on from the high conductivities observed for samples doped with Mg on the Si site, three additional Mg doped samples, co-doped with either Ba, B or Ga [$\text{La}_{9.33}\text{Ba}_{0.5}\text{Si}_{5.5}\text{Mg}_{0.5}\text{O}_{26}$, $\text{La}_{9.83}\text{Si}_5\text{Mg}_{0.5}\text{O}_{26}$ ($M=\text{B}, \text{Ga}$)] were prepared to see if further improvements in the conductivity could be achieved. Bulk conductivity data for these three samples are shown in Table 3. This data shows that all three co-doped samples have similar high conductivities to the singly doped $\text{La}_{9.67}\text{Si}_{5.5}\text{Mg}_{0.5}\text{O}_{26}$. An interesting comparison can be made between the Ba- and Mg-doped sample $\text{La}_{9.33}\text{Ba}_{0.5}\text{Si}_{5.5}\text{Mg}_{0.5}\text{O}_{26}$ and the dual-site Mg-doped sample, $\text{La}_{9.33}\text{Mg}_{0.5}\text{Si}_{5.5}\text{Mg}_{0.5}\text{O}_{26}$ (Tables 2 and 3). This shows that co-doping $\text{La}_{9.67}\text{Si}_{5.5}\text{Mg}_{0.5}\text{O}_{26}$ with Ba results in no major change in conductivity, while co-doping Mg on the La site reduces the conductivity by an order of magnitude. This difference can be correlated with the cation size effects on the La site outlined above.

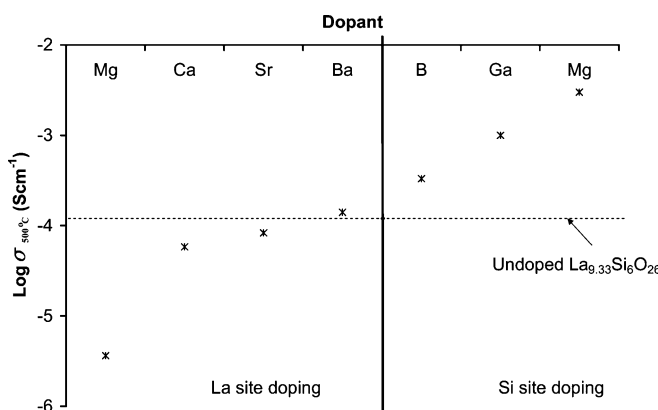


Fig. 3 Comparison of the conductivities at 500 °C of samples with the same level of cation vacancies (cation vacancy level=0.33), but with differing dopants: La site doping; compositions= $\text{La}_{8.67}\text{MSi}_6\text{O}_{26}$ ($M=\text{Mg}, \text{Ca}, \text{Sr}, \text{Ba}$); Si site doping; compositions= $\text{La}_{9.67}\text{Si}_5\text{MO}_{26}$ ($M=\text{B}, \text{Ga}$), $\text{La}_{9.67}\text{Si}_{5.5}\text{Mg}_{0.5}\text{O}_{26}$

Table 3 Conductivity data for $\text{La}_{9.67}\text{Si}_{5.5}\text{Mg}_{0.5}\text{O}_{26}$ co-doped with Ba, B and Ga

Sample composition	σ (Scm $^{-1}$) at 500 °C	E_a (eV)
$\text{La}_{9.33}\text{Ba}_{0.5}\text{Si}_{5.5}\text{Mg}_{0.5}\text{O}_{26}$	1.8×10^{-3}	0.62
$\text{La}_{9.83}\text{Si}_5\text{Mg}_{0.5}\text{B}_{0.5}\text{O}_{26}$	1.9×10^{-3}	0.63
$\text{La}_{9.83}\text{Si}_5\text{Mg}_{0.5}\text{Ga}_{0.5}\text{O}_{26}$	3.1×10^{-3}	0.71

In summary, from the doping studies reported, the following conclusions can be made.

1. The incorporation of low levels of lower valent dopants ($\text{B}^{3+}, \text{Ga}^{3+}, \text{Mg}^{2+}, \text{Zn}^{2+}$) on the Si site results in a significant increase in the oxide ion conductivity.
2. The influence of lower-valent dopants on the La site is strongly affected by the size of the dopant, with low levels of larger dopants, e.g. Ba^{2+} , producing little change in conductivity, while smaller dopants, e.g. Mg^{2+} , result in a significant reduction in conductivity. This can be attributed to the effect on the local structure of a change in coordination from 9 coordination for large dopants to 6 coordination for small dopants.

Overall, the strong influence of Si site doping on the conductivity provides further support to modelling predictions that the silicate sublattice plays a critical role in the conduction process.

Mg, Ga doping in $\text{Ln}_{9.33}\text{Si}_6\text{O}_{26}$: effect of rare-earth size

Following the initial positive results that doping with Ga and Mg on the Si site in $\text{La}_{9.33}\text{Si}_6\text{O}_{26}$ leads to a significant increase in conductivity, we decided to investigate whether this conductivity enhancement was influenced by the rare-earth size. With this in mind, we attempted the synthesis of the phases $\text{Ln}_{9.33}\text{Si}_6\text{O}_{26}$, $\text{Ln}_{9.67}\text{Si}_5\text{GaO}_{26}$, $\text{Ln}_{9.5}\text{Si}_{5.75}\text{Mg}_{0.25}\text{O}_{26}$ ($\text{Ln}=\text{La}, \text{Pr}, \text{Nd}, \text{Sm}, \text{Eu}, \text{Gd}$). The first two systems were successfully prepared for the complete range of rare earth elements studied. In contrast, it has so far not proved possible to prepare single-phase Mg-doped samples, $\text{Ln}_{9.5}\text{Si}_{5.75}\text{Mg}_{0.25}\text{O}_{26}$, for rare earth elements smaller than Pr. This suggests that as the rare-earth size decreases, the structure cannot cope with the local distortions introduced in replacing Si^{4+} with the much larger Mg^{2+} ion. Further discussion will, therefore, focus on the first two systems, $\text{Ln}_{9.33}\text{Si}_6\text{O}_{26}$ and $\text{Ln}_{9.67}\text{Si}_5\text{GaO}_{26}$.

The bulk conductivities for these samples are given in Tables 4a and 4b. From these data, it can be seen that the conductivities of the undoped $\text{Ln}_{9.33}\text{Si}_6\text{O}_{26}$ system are similar for the larger rare earth elements La, Pr, Nd, while as the rare-earth size decreases further, there is a decrease in the low-temperature conductivity along with an increase in the activation energy (Fig. 4a). These results, therefore, indicate that the size of the rare earth element has a significant influence on the oxide ion conduction, in line with previous reports [3], with the highest conductivities observed for the largest rare earth element, the conductivity

at 500°C of $\text{La}_{0.33}\text{Si}_6\text{O}_{26}$ being two orders of magnitude higher than that of $\text{Gd}_{0.33}\text{Si}_6\text{O}_{26}$.

For the Ga-doped samples, $\text{Ln}_{0.67}\text{Si}_5\text{GaO}_{26}$, the rare-earth size has an even larger effect on the conductivity (Table 4b), with a clear decrease in the conductivity at 500°C and increase in activation energy as the rare-earth size decreases. If the data is plotted vs rare-earth ionic radius (Fig. 4b), it can be seen that there is a clear correlation between conductivity/activation energy and rare-earth cation radius. Thus, although the conductivities of the undoped systems $\text{Ln}_{0.33}\text{Si}_6\text{O}_{26}$ ($\text{Ln}=\text{La}, \text{Pr}, \text{Nd}$) are similar, on Ga doping to form $\text{Ln}_{0.67}\text{Si}_5\text{GaO}_{26}$, significant differences are observed, with the conductivities for $\text{Ln}=\text{Pr}, \text{Nd}$ being noticeably lower than for $\text{Ln}=\text{La}$.

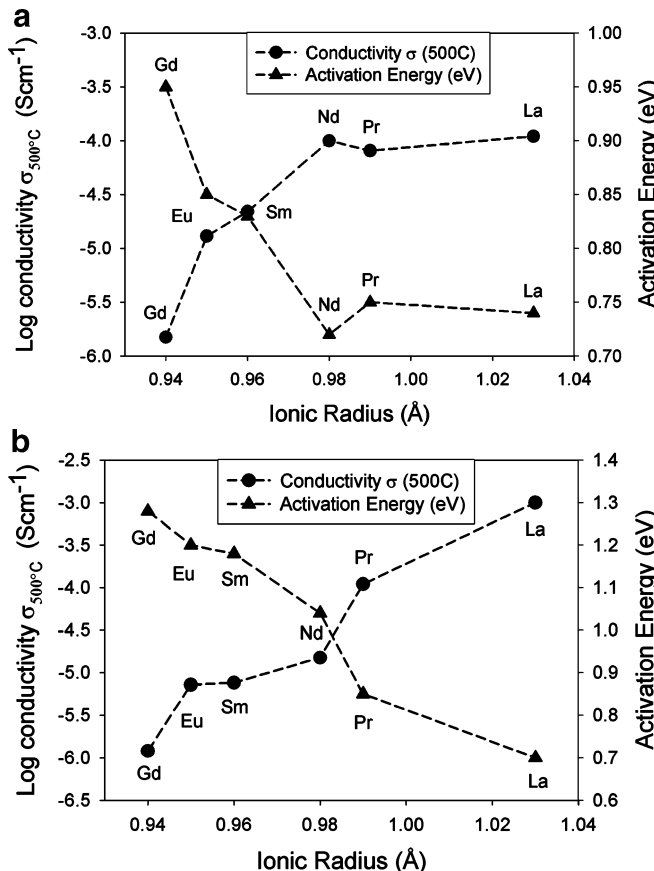


Fig. 4 Variation of conductivity at 500 °C/activation energy vs rare-earth cation size for **a** $\text{Ln}_{0.33}\text{Si}_6\text{O}_{26}$, **b** $\text{Ln}_{0.67}\text{Si}_5\text{GaO}_{26}$ ($\text{Ln}=\text{rare earth}$)

Table 4a Conductivity data for $\text{Ln}_{0.33}\text{Si}_6\text{O}_{26}$

Sample composition	σ (Scm $^{-1}$) at 500 °C	E_a (eV)
$\text{La}_{0.33}\text{Si}_6\text{O}_{26}$	1.1×10^{-4}	0.74
$\text{Pr}_{0.33}\text{Si}_6\text{O}_{26}$	8.1×10^{-5}	0.75
$\text{Nd}_{0.33}\text{Si}_6\text{O}_{26}$	1.0×10^{-4}	0.72
$\text{Sm}_{0.33}\text{Si}_6\text{O}_{26}$	2.2×10^{-5}	0.83
$\text{Eu}_{0.33}\text{Si}_6\text{O}_{26}$	1.3×10^{-5}	0.85
$\text{Gd}_{0.33}\text{Si}_6\text{O}_{26}$	1.5×10^{-6}	0.95

Table 4b Conductivity data for $\text{Ln}_{0.67}\text{Si}_5\text{GaO}_{26}$

Sample composition	σ (Scm $^{-1}$) at 500°C	E_a (eV)
$\text{La}_{0.67}\text{Si}_5\text{GaO}_{26}$	1.0×10^{-3}	0.70
$\text{Pr}_{0.67}\text{Si}_5\text{GaO}_{26}$	1.1×10^{-4}	0.85
$\text{Nd}_{0.67}\text{Si}_5\text{GaO}_{26}$	1.5×10^{-5}	1.04
$\text{Sm}_{0.67}\text{Si}_5\text{GaO}_{26}$	7.6×10^{-6}	1.18
$\text{Eu}_{0.67}\text{Si}_5\text{GaO}_{26}$	7.2×10^{-6}	1.20
$\text{Gd}_{0.67}\text{Si}_5\text{GaO}_{26}$	1.2×10^{-6}	1.28

A comparison of the data between $\text{Ln}_{0.33}\text{Si}_6\text{O}_{26}$ and $\text{Ln}_{0.67}\text{Si}_5\text{GaO}_{26}$ samples shows that, although for $\text{Ln}=\text{La}$ the Ga doping leads to a substantial (an order of magnitude) increase in conductivity (as reported above), this is not observed for the smaller rare earth elements. In contrast, a decrease in the conductivity at 500 °C is observed in most cases, e.g. for $\text{Ln}=\text{Nd}$, the conductivity at this temperature decreases by an order of magnitude on doping with Ga to give $\text{Nd}_{0.67}\text{Si}_5\text{GaO}_{26}$.

The key change on reducing the size of the rare earth is a significant increase in the activation energy on Ga doping. Two possible explanations could account for this increase in activation energy:

1. A reduction in the oxygen interstitial concentration, with the higher activation energy correlated with a combination of the energy to create these oxygen interstitials and the energy for their migration.
2. The interstitial oxygen ions are still present, but the Ga doping either affects the conduction pathway resulting in a higher migration energy or mediates “trapping” of the interstitial ions, so that an additional contribution to the activation energy is required to free them.

Of the two possibilities, explanation 2 appears the most logical, as Ga doping will lead to a considerable expansion of the tetrahedra, and so blocking of the conduction pathway and/or “trapping” effects on Ga doping might reasonably be expected. In this respect, it is relevant to note that Ti doping for Si has been recently reported, leading to a dramatic reduction in conductivity and increase in activation energy, even for samples containing oxygen excess, which has been attributed to trapping of the interstitial oxygens [37]. However, the above argument does not explain why, for the largest rare earth (La), an increase in conductivity is observed on Ga doping. In this particular case, modelling studies have suggested that the local distortions accompanying the Ga incorporation are accommodated more by the La positions than the oxygen channels [33], thus, keeping these channels open for conduction. It seems likely, however, that this process could be affected by a reduction in the rare-earth size, such that there becomes a point when the local distortion may no longer be accommodated by the rare-earth positions. In such a situation, the induced local distortions on Ga incorporation may begin to significantly affect the oxygen channels and, therefore, reduce the conductivity. In this respect, it would be interesting to perform further modelling studies on smaller rare-earth apatite systems.

In summary, the results show that the effect of dopants on the conductivity of apatite-type ionic conductors can be strongly influenced by the rare-earth cation size.

Acknowledgement We would like to thank the Engineering and Physical Sciences Research Council for funding this study.

References

1. Goodenough JB (2003) *Annu Rev Mater Res* 33:91
2. Nakayama S, Aono H, Sadaoka Y (1995) *Chem Lett* 431
3. Nakayama S, Sakamoto M (1998) *J Eur Ceram Soc* 18:1413
4. Nakayama S, Sakamoto M, Higuchi M, Kodaira K, Sato M, Kakita S, Suzuki T, Itoh K (1999) *J Eur Ceram Soc* 19:507
5. Higuchi M, Katase H, Kodaira K, Nakayama S (2000) *J Cryst Growth* 218:218
6. Nakayama S, Sakamoto M, Higuchi M, Kodaira K (2000) *J Mater Sci Lett* 19:91
7. Nakayama S, Higuchi M (2001) *J Mater Sci Lett* 20:913
8. Tao S, Irvine JTS (2001) *Mater Res Bull* 36:1245
9. Sansom JEH, Richings D, Slater PR (2001) *Solid State Ionics* 139:205
10. Arikawa H, Nishiguchi H, Ishihara T, Takita Y (2000) *Solid State Ionics* 136–137:31
11. Sansom JEH, Hildebrandt L, Slater PR (2002) *Ionics* 8:155
12. Nakayama S, Sakamoto M (2001) *J Mater Sci Lett* 20:1627
13. Berastegui P, Hull S, Garcia Garcia FJ, Grins J (2002) *J Solid State Chem* 168:294
14. Leon-Reina L, Martin-Sedeno ME, Losilla ER, Caberza A, Martinez-Lara M, Bruque S, Marques FMB, Sheptyakov DV, Aranda MAG (2003) *Chem Mater* 15:2099
15. Abram EJ, Kirk CA, Sinclair DC, West AR (2005) *Solid State Ionics* 176:1941
16. Masubuchi Y, Higuchi M, Kikkawa S, Kodaira K, Nakayama S (2004) *Solid State Ionics* 175:357
17. Slater PR, Sansom JEH (2003) *Solid State Phenomena* 90–91:195
18. Masubuchi Y, Higuchi M, Katase H, Takeda T, Kikkawa S, Kodaira K, Nakayama S (2004) *Solid State Ionics* 166:213
19. Islam MS, Tolchard JR, Slater PR (2003) *Chem Commun* 1486
20. Tolchard JR, Islam MS, Slater PR (2003) *J Mater Chem* 13:1956
21. Leon-Reina L, Losilla ER, Martinez-Lara M, Bruque S, Aranda MAG (2004) *J Mater Chem* 14:1142
22. Leon-Reina L, Losilla ER, Martinez-Lara M, Martin-Sedeno MC, Bruque S, Nunez P, Sheptyakov DV, Aranda MAG (2005) *Chem Mater* 17:596
23. Leon-Reina L, Losilla ER, Martinez-Lara M, Bruque S, Llobet A, Sheptyakov DV, Aranda MAG (2005) *J Mater Chem* 15:2489
24. Sansom JEH, Tolchard JR, Apperley D, Islam MS, Slater PR (2006) *J Mater Chem* DOI 10.1039/b600122j
25. Abram EJ, Sinclair DC, West AR (2001) *J Mater Chem* 11:1978
26. McFarlane J, Barth S, Swaffer M, Sansom JEH, Slater PR (2002) *Ionics* 8:149
27. Tolchard JR, Sansom JEH, Slater PR, Islam MS (2004) *Solid State Ionics* 167:17
28. Shaula AL, Kharton VV, Patrakeev MV, Waerenborgh JC, Rojas DP, Vyshatko NP, Tsipis EV, Yaremchenko AA, Marques FMB (2004) *Mater Res Bull* 39:763
29. Yaremchenko AA, Shaula AL, Kharton VV, Waerenborgh JC, Rojas DP, Patrakeev MV, Marques FMB (2004) *Solid State Ionics* 171:51
30. Najib A, Sansom JEH, Tolchard JR, Islam MS, Slater PR (2004) *Dalton Trans* 19:3106
31. Kharton VV, Shaula AL, Patrakeev MV, Waerenborgh JC, Rojas DP, Vyshatko NP, Tsipis EV, Yaremchenko AA, Marques FMB (2004) *J Electrochem Soc* 151:A1236
32. Tolchard JR, Sansom JEH, Islam MS, Slater PR (2005) *Dalton Trans* 20:1273
33. Tolchard JR, Slater PR, Islam MS (2006) *J Am Chem Soc* (in press)
34. Yoshioka H, Tanase S (2005) *Solid State Ionics* 176:2395
35. Yoshioka H (2004) *Chem Lett* 33:392
36. Sansom JEH, Slater PR (2002) *Proceedings of the 5th Euro SOFC forum* 2:627
37. Sansom JEH, Sermon PA, Slater PR (2005) *Solid State Ionics* 176:1765